One- and two-electron transitions in slow C^{5+}-He collisions: Total and angle-differential cross sections and coherence parameters

Wolfgang Fritsch
Bereich Theoretische Physik, Hahn-Meitner-Institut Berlin, D-14109 Berlin, Germany

C. D. Lin
Institute of Physics, National Chiao-Tung University, Taiwan
and Department of Physics, Kansas State University, Manhattan, Kansas 66506

(Received 24 April 1996)

Transitions of one or two electrons in C^{5+}-He collisions are studied within the semiclassical close-coupling description of atomic collisions, at impact energies of 1–35 keV/u. Angle-integrated cross sections are determined for single-transfer, double-transfer, and transfer-excitation channels. For single capture to $3p$ states and for two final states in the two-electron transfer channel, angle-differential cross sections are derived and a number of coherence parameters that depend on the quantum-mechanical phases are calculated. The results are compared with recent data on angle-differential two-electron transfer and with results from an earlier theoretical study. [S1050-2947(96)03311-2]

PACS number(s): 34.70.+e, 32.80.Dz

I. INTRODUCTION

In studies of slow atomic collisions, it is probably the most ambitious task to understand the details of weak transitions. Recent experiments on the C^{5+}-He system have determined the weak population of doubly excited $2l2l'\ ^1L$ states in two-electron capture [1,2], the population of magnetic substates in these transitions [2], and most recently [3] the angle-differential population of these substates, as well as the angle dependence of certain density matrices or coherence parameters that are sensitive to the quantum-mechanical phases of the scattering amplitudes. While such an experiment is challenging enough, its interpretation by theory compounds a number of difficulties, such as (i) the description of *weak transitions in a two-electron system* that compete with strong one-electron transitions, (ii) the determination of *angle-differential* quantities in a system with a nontrivial connection between impact parameters and scattering angles, and (iii) the derivation of elements of the density matrix that depend on the *phases* of transition amplitudes.

In this work we study the C^{5+}-He system within the semiclassical close-coupling description of atomic collisions, with the aim of understanding the primary features of this system as well as the finer details as brought out by recent measurements [3]. The theoretical description is an extension of our own earlier work on Be^{4+}-He and B^{4+}-He collisions [4], as well as work by Hansen and Taulbjerg [5] on a few A^{q+}-He systems, in both of which angle-differential results are not considered. The determination of phase-dependent quantities in this work represents also an extension of the scope of the work by Harel and Jouin [6] within the molecular-orbital description, in which total and differential cross sections for various channels in N^{7+}-He collisions are studied.

In the next section we present the theory as we use it in this work to describe slow C^{5+}-He collisions. In Sec. III, the calculated results are presented and discussed. The conclusions of this work are summarized in Sec. IV. We use atomic units unless stated otherwise.

II. THEORY

The general features of the semiclassical close-coupling theory of atomic collisions are discussed in Ref. [7]. For the discussion of the energies of the system and for the derivation of integrated cross sections, we use the same form of the theory as in our earlier work [4] on similar systems; see Sec. II A. In Sec. II B, we discuss the evaluation of angle-differential cross sections.

A. Choice of the Hamiltonian and the basis SA

The nuclei are assumed to move on rectilinear classical trajectories. The core electron of the C^{5+} projectile is assumed to stay inert in the collision; its action is embodied in the choice of a non-Coulombic projectile potential

$$V_C(r) = -\frac{5}{r} - \frac{1}{r}\frac{1}{Kd[\exp(r/d)-1]+1}, \qquad (1)$$

with r the electron coordinate and parameters K and d as taken from Ref. [8]. With this potential, and with the potential $V_{He} = -2/r$ of the bare target nucleus acting on the two active electrons, the two-electron Hamiltonian is constructed. The basis for the representation of the electron dynamics consists of antisymmetrized, binary products of single-electron hydrogenlike orbitals, just like in our earlier work [4]. In the basis, we include (i) one target centered configuration that represents the He ground state, (ii) a few projectile centered configurations that represent the double capture states of C^{3+}, and (iii) two-center configurations with one electron at the target and the other at the projectile, which represent single capture states ($nlm\ C^{4+}$, $1s\ He^+$) and also transfer-excitation states ($nlm\ C^{4+}$, $2l'm'\ He^+$, $l' = 0,1$). The He ground state is represented by a configuration of type

TABLE I. Projectile-centered two-electron configurations used in this work to represent the states of $1snln'l'$ C^{3+} after two-electron transfer in $C^{5+}(1s)$-He collisions. Given are the parameters $(n_1 l_1 \rho_1\ n_2 l_2 \rho_2)$ of hydrogenic orbitals, with ρ the charge number of the orbital, the classification as to the total angular momentum L, and the two-electron binding energy ϵ (in atomic units) of the state. The binding energies $\epsilon_{\rm HT}$ from the work by Hansen and Taulbjerg [5] are given in the last column.

n_1	l_1	ρ_1	n_2	l_2	ρ_2	NL	ϵ	$\epsilon_{\rm HT}$
1	0	6.41	1	0	4.29	$1\,^1S$		
1	0	5.70	2	0	4.55	$2\,^1S$		
1	0	5.72	2	1	3.98	$2\,^1P$		
1	0	5.70	3	2	4.00	$3\,^1D$		
2	0	5.25	2	0	5.25	^1S	−5.94	−5.93
2	1	4.83	2	0	5.11	^1P	−5.47	−5.50
2	1	4.69	2	1	4.69	^1D	−5.40	−5.39
2	1	4.64	2	1	4.64	^1S	−5.14	−5.15
3	0	4.86	3	0	4.86	^1S		

$1s\rho\ 1s\rho'$ with a pair of charge numbers ρ and ρ' of 2.183 and 1.188. These charge numbers are derived in an optimization procedure, by minimizing the ground-state energy of helium with respect to a variation of the charge numbers. Similar procedures have been applied for defining the charge numbers for the other states in the basis; for an earlier application see also the basis choice in the work on He^+-H collisions [9]. The other basis configurations are given in Tables I and II. The energies in Table I are binding energies of the two active electrons, the energies in Table II are the binding energies of the transferred electron. *Two-electron* binding energies are determined, in the one-electron transfer channel, by adding to the energies in Table II the number -2, the energy of the He^+ $1s$ configuration. In the transfer-excitation channel, the number -0.5 has to be added, i.e., the energy of the He^+ $2l$ configuration. Including the multiplicity of the magnetic quantum number, the basis consists of 15 double-transfer configurations, 11 single-transfer configurations, and 33 transfer-excitation configurations.

There is fair quantitative agreement between the binding energies of this work and of the work by Hansen and Taulbjerg [5], who employ a purely Coulombic potential at the carbon center. There is also good agreement for the energy (-2.88 a.u.) of the He ground state, although Hansen and Taulbjerg allow also for a small $2p^2$-type contribution in this wave function. The largest discrepancy between calculated binding energies is for the single-capture $2s,2p$ states; cf. Table II. This seems, however, still tolerable since the calculated binding energies from both descriptions are in turn bracketed by the experimental energies for the two possible spin orientations, singlet or triplet, with respect to the spin of the inert core electron. Including the spin interaction with the core electron lies beyond the scope of this description. The uncertainty thus introduced into the calculated transition cross sections is hence larger than the uncertainty caused by ambiguities of the chosen potential or the chosen basis.

TABLE II. Basis states for describing the $1snl$ C^{4+} states after transfer of one electron in $C^{5+}(1s)$-He collisions. Given are the parameters $(nl\rho)$ of hydrogenic orbitals and the binding energy ϵ (in atomic units) of the outer electron. The energies from the work by Hansen and Taulbjerg [5] are designated $\epsilon_{\rm HT}$. The last two columns list the corresponding experimental binding energies [10] for the singlet (S) and triplet (T) combination of the electron spins in C^{4+}.

n	l	ρ	ϵ	$\epsilon_{\rm HT}$	S	T
1	0	6.04				
2	0	5.13	−3.32	−3.37	−3.22	−3.42
2	1	5.10	−3.15	−3.19	−3.09	−3.22
3	0	5.17	−1.44	−1.39	−1.42	−1.47
3	1	5.05	−1.40	−1.39	−1.38	−1.42
3	2	5.00	−1.39	−1.39	−1.39	−1.39
1	0	2.57				

From the energies of the one-electron capture states in Table II one notes that the dominant channel, the one-electron capture channel to the $n=3$ C^{4+} states, is very close, energetically, to the transfer-excitation channel to the $n=2$ C^{4+} states (with the target left as $2s$ or $2p$ He^+), with *two-electron* energies of, respectively, -3.44 a.u. and -3.82 a.u. for the $l=0$ states. For this very reason transfer-excitation states are included in the dynamical calculations. At low energies and small impact parameters, their population may become comparable to the population of single transfer states; they may also act as a medium for populating the weak double-transfer states in slow collisions.

B. Determination of differential cross sections SB

The angle-differential cross section for an inelastic transition from an initial state i to a final state f can be written as the square of a scattering amplitude A_{fi} at an angle θ,

$$d\sigma_{fi}/d\theta = 2\pi \sin\theta |A_{fi}|^2. \tag{2}$$

The scattering amplitudes A_{fi} in Eq. (2) may be determined in turn from impact-parameter-dependent transition amplitudes c_{fi}, starting from the semiclassical approximation and the eikonal approach. The formalism has been described and implemented in a number of investigations; see, e.g., Ref. [11] and references therein. Here we present our own implementation very briefly, with emphasis on the difficulties that arise in a study at low collision energy involving multiply charged ions.

The scattering amplitude A_{fi} in Eq. (2) is given [12] by

$$A_{fi}(\theta) = \mu v (-i)^{|m_f - m_i|+1} \times \int_0^\infty b\, db J_{|m_f-m_i|}(\eta b) c_{fi}(b,+\infty). \tag{3}$$

Here μ is the reduced mass, v is the relative collision velocity, and m_f (m_i) is the magnetic quantum number of the final (intial) state. The function J designates a Bessel function of the first kind, with $\eta = 2\mu v \sin(\theta/2)$, and $c(b,+\infty)$ is the ''semiclassical'' scattering amplitude that is evaluated for a given impact parameter b at time $t\to\infty$ or $z = vt \to \infty$.

Equation (3) is essentially a diffraction integral that accounts for the contributions from all impact parameters to the scattering amplitude at a given angle. Its numerical evaluation poses a number of difficulties since both the Bessel

function and the scattering amplitude are oscillatory functions of impact parameter b. For the slow collisions considered here, the oscillations due to the scattering amplitude are very rapid.

The scattering amplitude c_{fi} in Eq. (3) can be separated into an electronic contribution that is obtained from solving the coupled equation for the transition amplitudes a_{fi} and the additional nuclear (or core ionic) contribution that is due to the Coulomb repulsion between the two nuclei. In the actual evaluation of the transition amplitudes a_{fi}, the core-core interaction is usually not considered and hence such separation of terms occurs naturally,

$$c_{fi}(b,+\infty)=a_{fi}(b,+\infty)\exp\left\{ i\frac{2}{v}Z_AZ_B\ln b\right\}. \tag{4}$$

In Eq. (4), Z_A and Z_B are the effective charges that define the Coulomb trajectory of the two colliding nuclei. For collisions involving multiply charged ions at low velocities, the phase from the second term in Eq. (4) is large and changes rapidly with impact parameter.

The determination of the phase of the electronic transition amplitude a_{fi} in Eq. (4) is not trivial since the asymptotic charge of the receding ion causes a fast variation of this phase with impact parameter. These amplitudes are determined numerically, as usual [7], for a mesh of impact parameters b and a fixed end point z_1 of the time integration; they are hence known as a set of complex numbers. By plotting the amplitudes over impact parameters, their phases can be determined, up to an overall multiple of 2π, provided that the mesh of impact parameters is sufficiently dense, i.e., provided that there are a few mesh points within each full cycle of the phase rotation. For slow collisions, this is very hard to achieve without further provisions, as it would require the consideration of many hundreds of impact parameters for each velocity.

At interatomic separations R where electronic transitions do not yet or no longer occur, the electron transition amplitude a_{fi} can be written as

$$a_{fi}(b,t)=a_{fi}^0\exp\left\{ -i\left[\epsilon_f t+\mathrm{sgn(t)}\ \frac{Z}{v}\ln(R-v|t|)\right]\right\} \tag{5}$$

where ϵ_f is the energy of state f, Z is the effective charge of the collision partner that causes the phase oscillation, and sgn (t) designates the sign of time t. Hence, when changing the end point of the time integration of the coupled equations from t_0 to t_1 (separations R_0 and R_1), a phase change of $Z_f/v\ln[\{R_1\text{-}vt_1\}/\{R_0\text{-}vt_0\}]$ is effected, where the purely time-dependent energy term has been dropped. A similar phase change, with an effective charge of Z_i, occurs when changing the initial point of the time integration. One can then express the phase $\phi(b,z_1)$ of the amplitude a_{fi} in Eq. (5) for given fixed initial and final points of the time integration $z_1=v|t_1|$, with reference to another point z_0, which, for convenience, is chosen to be $z_0=0$,

$$\phi(b,z_1)=\phi(b,z_0)-\frac{Z_i+Z_f}{v}\ln\left\{ \sqrt{\frac{z_1^2}{b^2}+1}-\frac{z_1}{b}\right\}. \tag{6}$$

We use Eq. (6) to facilitate the determination of the phase ϕ of the amplitude a_{fi} from the coupled equations. Shifting the end point of the integration, with the help of Eq. (6), changes the speed of the oscillations of the phase with impact parameters. It turns out that the oscillations are less rapid at small impact parameters when a small value of z_1 is chosen. Likewise, the oscillations are less rapid at large impact parameters when a large value of z_1 is chosen. Once the full set of phases for the mesh of impact parameters is known it can be transformed to any desired common end point of the time integration.

For $z_1\gg b$, the logarithmic term in Eq. (6) can be simplified to $\ln(b/2z_1)$. The phase of the scattering amplitude Eq. (4) can hence be written as

$$\phi(b,z_0)+\frac{2Z_AZ_B-(Z_i+Z_f)}{v}\ln b, \tag{7}$$

where only terms that depend on the impact parameter have been kept. Here $Z_i=10$ for the present system since both electrons in the He initial state ''see,'' at large separations, the Coulomb field of a charge with charge number 5. Similarly, for double capture, $Z_f=4$. For single capture and for transfer excitation, the receding ions give rise to a contribution of $5+2=7$ to the charge number of the logarithmic phase dependence in Eq. (5), but the electron-electron interaction leads to another term of -1, adding up to $Z_f=6$ for these channels.

In order to perform the integration in Eq. (3) numerically, we first divide the range of impact parameters b into small sectors where within each sector the integrand can be written in the form

$$F(b)\exp\{iw\ln b\}, \tag{8}$$

i.e., we try to factor out the logarithmic impact-parameter dependence of the phase; see expression (7). To evaluate the integral over the sector, we substitute $x=\ln b$ and rewrite the integral in the form

$$\int_{x_n}^{x_{n+1}}dx(ax^2+bx+c)e^{iwx}, \tag{9}$$

where we have fitted the function $F(b)$ within the sector by a quadratic function. The integration over this sector is then carried out analytically. It is of course important to make sure that within each sector the function $F(b)$ is a smooth function of $x=\ln b$. The accuracy of the procedure can be checked by changing the size of the sectors. In another check on the accuracy one can integrate the differential cross sections over angles and compare the cross section with the result obtained from integrating the probabilities over impact parameters.

C. Evaluation of coherence parameters

From the scattering amplitudes for the different final magnetic substates, one can extract the phase information or, in general, the coherence parameters. We concentrate here on the P states.

For the P states, the two scattering amplitudes A_m for $m=0$ and $m=1$ (the amplitude for $m=-1$ and $m=+1$ are

identical since the quantization axis is chosen to be along the beam direction) give four real parameters. Since the overall phase is not important, there are three real parameters to be determined. From the scattering amplitudes these three parameters can be chosen as (i) the total differential cross section $|A_0|^2+2|A_1|^2$, (ii) the fraction λ_0 of the $m=0$ component,

$$\lambda_0=|A_0|^2/(|A_0|^2+2|A_1|^2), \tag{10}$$

and (iii) the phase difference β_{01},

$$\beta_{01}=\beta_0-\beta_1, \tag{11}$$

between the two amplitudes A_m for $m=0$ and $m=1$. The fraction λ_0 and the phase difference β_{01} do not have obvious classical interpretation. For the P state, two other quantities, the orientation parameter and the alignment angle, are often used.

For the D state, we will use later also the fraction λ_2 of the $m=2$ component,

$$\lambda_2=2|A_2|^2/(|A_0|^2+2|A_1|^2+2|A_2|^2), \tag{12}$$

along with the fraction λ_0, which is defined as for the P state Eq. (10), but with the probability of populating the D state in the denominator as in Eq. (12). In our calculation the incident beam direction is chosen to be the quantization axis, the collision plane is the x-z plane with the incident particle entering the collision on the $+x$ side. The y axis is chosen such that x-y-z forms a right-handed coordinate system. In this coordinate frame, the orientation parameter $L_\perp$ for the P state is given by

$$L_\perp=2\sqrt{2}\,\mathrm{Im}(\,A_0A_1^*)/\sigma_\mathrm{T} \tag{13}$$

and for the D state it is

$$L_\perp=2\sqrt{6}\,\mathrm{Im}(A_0A_1^*)/\sigma_\mathrm{T}+4\,\mathrm{Im}(A_1A_2^*)/\sigma_\mathrm{T}, \tag{14}$$

where σ_T is the total cross section summed over all magnetic quantum numbers.

In discussing the coherent parameters the explicit expressions depend on the choice of a coordinate frame. In order to compare with quantities quoted in the experimental paper by Khemliche *et al.* [3], we note that they chose the y-z plane as the collision plane, with $+z$ as the beam direction but with $+y$ corresponding to our $+x$ direction. Thus the phase angles in their scattering amplitudes are 90° and 180° behind ours for, respectively, the $m=1$ and $m=2$ components. Transforming to their coordinate frame, the expression for $L_\perp$ for the P state is

$$L_\perp=-2\sqrt{2}|A_0||A_1|\cos\beta_{01}, \tag{15}$$

where now the phase angles are defined in the frame of Khemliche *et al.* [3]. In order to avoid confusion, we will henceforth use their frame of reference whenever referring to the phase angles in this work.

III. RESULTS AND DISCUSSION

In this section we present the results of the calculations for the integrated cross sections for the various final states and also the results for the differential cross sections and coherence parameters. We start in Sec. III A with an overview of the processes in C^{5+}-He collisions, giving molecular energies, total transfer cross sections, and one sample of the impact parameter dependence of transitions. We then proceed in Sec. III B to a closer discussion of total cross sections for single-electron transfer, two-electron transfer, and transfer excitation, and, in Sec. III C, of differential cross sections and coherence parameters.

A. Overview of transitions

1. Molecular energies

In slow collisions, the mechanisms of electron transitions can be visualized in a consideration of the molecular-orbital (MO) energies. In Fig. 1 we show the two-electron energies of Σ and Π states, as they result from a diagonalization of the two-center two-electron Hamiltonian of the system within the basis of two-electron atomic configurations used in the close-coupling calculation. An extra line is drawn as an estimate of a ''diabatic'' state that correlates with the He ground state. This has been determined as the expectation value of the same Hamiltonian in the configuration of the He ground state. In the diagonalization, the Π states that correlate to transfer excitation states have been left out.

Figure 1 shows that the single-transfer states of $n=3$ in C^{4+}, where the target is left with the $1s$ He^+ state, are populated strongly at impact parameters below some 10 a.u. These states are only a little less bound than the combination of $n=2$ C^{4+} and $n=2$ He^+ states, which are populated, from the initial state, by transfer excitation at separations below some 6 a.u. Below impact parameters of about 3 a.u., two-electron capture states are populated by direct couplings with the initial He ground state. Below some 2 a.u., the avoided crossings may allow the population of double-capture states through coupling with single-capture states. Here, besides the radial couplings among the Σ states, Π-Π radial and Π-Σ rotational couplings may contribute to the population of double-capture states.

For a quantitative assessment of the importance of couplings, one would have to compute the corresponding nonadiabatic coupling matrix elements between MO configurations. However, this has not been done here since one would have to follow the coupling matrix elements of many pairs of potential curves and still the interpretation would not be transparent. We will show later that the calculated cross sections and the impact-parameter dependences of transition probabilities are consistent with the MO diagram and its interpretation.

2. Cross sections in C^{5+}-He collisions

An overview of the calculated total cross sections is given in Fig. 2. It shows that the dominant channel is the single-electron capture channel to the $n=3$ states and that it agrees closely, at low energies, with the measured total electron-capture cross section [13]. Single-electron capture to the $n=2$ states is much weaker. The major portion of the popu-

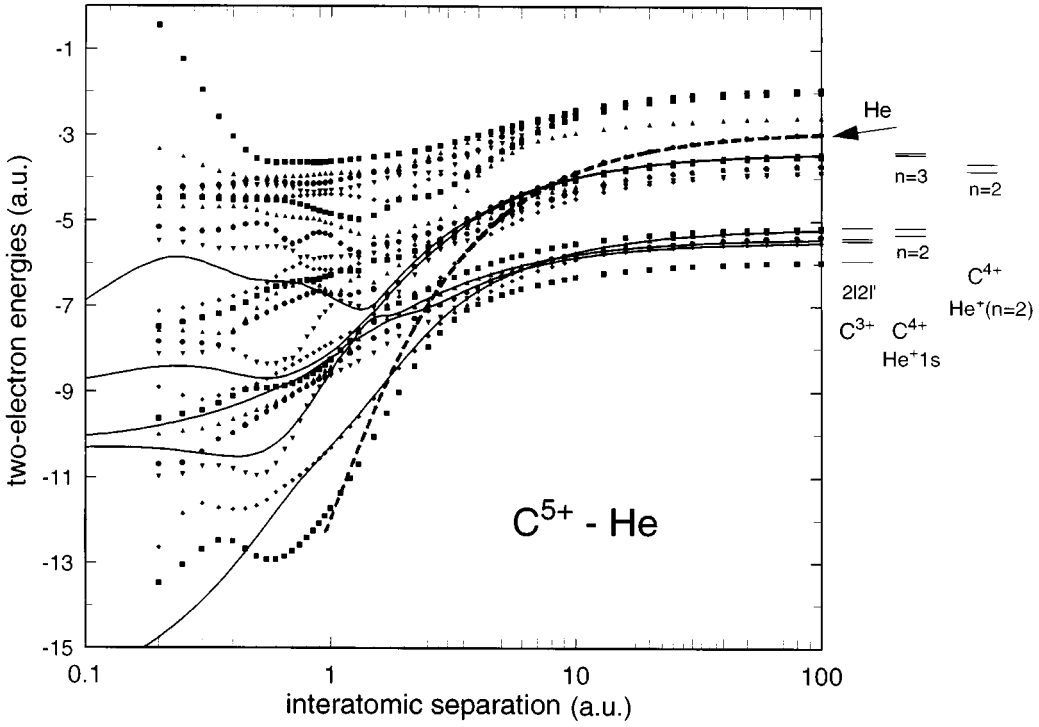

FIG. 1. Molecular energies of Σ (dots) and of Π (solid lines) two-electron configurations in the C^{5+}-He system. The broken line marks the course of a diabatic configuration that correlates to the He ground state. The levels outside the frame of the energy diagram mark the most important levels in, from left to right, two-electron transfer, in one-electron transfer, and in transfer excitation.

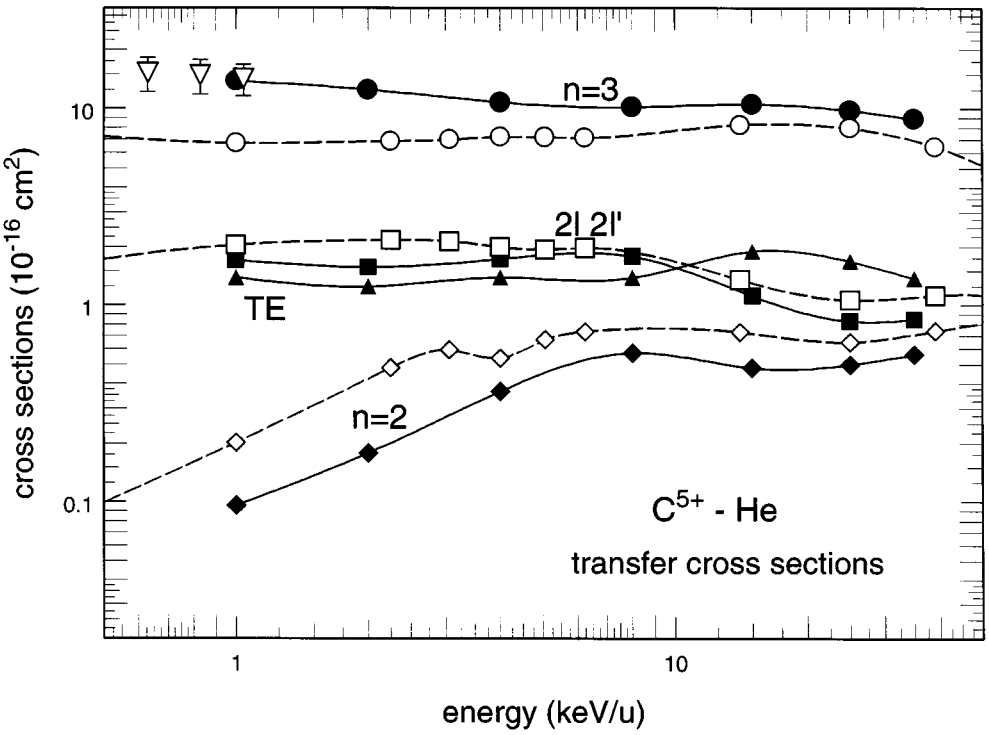

FIG. 2. Calculated cross sections for the C^{5+}-He collision system. Shown are the one-electron transfer cross sections, from this work, for the final C^{4+} $n=3$ (●) and $n=2$ (♦) shells, the two-electron transfer cross sections for the set of C^{3+} $2l2l'$ configurations (■), and the transfer-excitation cross section to the C^{4+} $n=2$, He^{+} $n=2$ configurations (▲). The corresponding results from the calculations by Hansen and Taulbjerg [5] are given as open symbols. The data by Iwai *et al.* [13] (▽) are for total one-electron transfer.

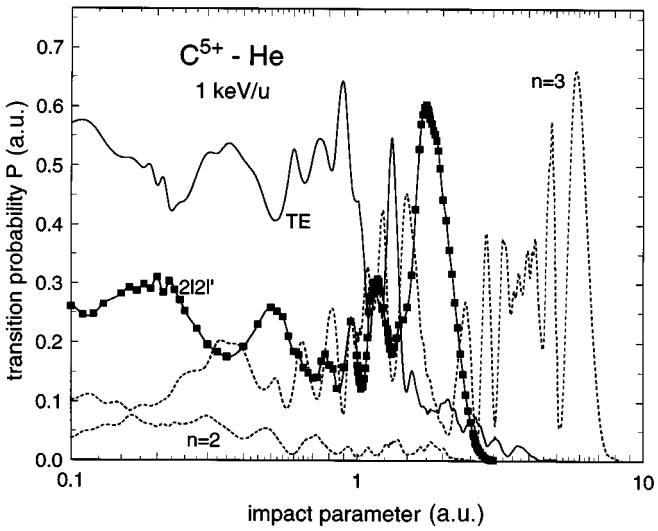

FIG. 3. Calculated transition probabilities in C^{5+}-He collisions at 1 keV/u. Shown are the probabilities for one-electron transfer to the $n=2$ and $n=3$ states in C^{4+} (dashed lines), for two-electron transfer to the $2l2l'$ configurations in C^{3+} (boxes), and for transfer excitation to C^{4+} $n=2$, He^{+} $n=2$ configurations (solid line).

lation of C^{4+} $n=2$ states, however, does not come from single capture to these states but from capture events that are accompanied, in a transfer-excitation process, by target excitation to the He^{+} $n=2$ states. The calculated cross section for total transfer excitation is of the same order as the cross section for double-electron capture to the C^{3+} $2l2l'$ configurations. For these total cross sections, the results from the calculations by Hansen and Taulbjerg [5] are qualitatively very similar to the results from this work, except for the process of transfer excitation, which has not been considered in Ref. [5].

3. Impact parameter dependence

For a better understanding of the relative magnitudes of cross sections, we show in Fig. 3 the calculated transition probabilities versus impact parameters at 1 keV/u. The impact-parameter dependence of all transition probabilities shows large oscillations as is typical for slow collisions with rapidly changing phase angles. The large cross sections for populating the $n=3$ states in one-electron transfer are seen to come mainly from contributions at large impact parameters $b \gtrsim 3$ a.u. The population of the $n=2$ states of C^{4+} through one-electron transfer is weak at all impact parameters. The probabilities for two-electron transfer have values in the range 0.2–0.3 below impact parameters of 3 a.u., but peak sharply at about an impact parameter of 1.8 a.u. It seems therefore that the double-transfer states are not merely populated directly from the initial states but also via the single-transfer states as a mediator, see the energy diagram in Fig. 1. The probabilities for transfer excitation are very large, around values of 0.5, at small impact parameters of 0.1–1.3 a.u., but become small beyond impact parameters of 2 a.u. Also these states are apparently populated, to a large extent, by multistep processes at small separations where a clear transition mechanism is not obvious. It is, however, very plausible to assume that the calculated probabilities for two-electron transfer are much influenced by the presence of transfer-excitation states. One would hence expect some difference in the calculated double-transfer cross sections between this work and the work by Hansen and Taulbjerg [5] as in the latter transfer excitation is not included.

TABLE III. Calculated partial transfer cross sections, in 10^{-16} cm^2, to the single capture C^{4+} nl states, in C^{5+}-He collisions. Note that the actual population of the $2l$ states is larger than shown here, through the process of transfer excitation; cf. later in this work.

E (keV/u)	2*s*	2*p*	3*s*	3*p*	3*d*
1.00	0.040	0.056	7.19	3.41	3.35
2.00	0.076	0.118	4.63	3.32	4.21
4.00	0.097	0.267	2.94	3.20	4.64
8.00	0.144	0.424	1.86	3.05	5.27
15.00	0.140	0.338	1.16	2.62	6.70
25.00	0.154	0.343	0.49	1.81	7.49
35.00	0.196	0.362	0.28	1.45	6.78

B. Total cross sections Results

1. Single-electron transfer

As shown in Fig. 2, single-electron capture to the $n=3$ states dominates in the energy range considered, while single capture to the $n=2$ states is much smaller. We list the calculated partial single-electron-capture cross sections in Table III for comparison with future studies.

The cross section for the dominant $3l$ channels are compared to the results from Hansen and Taulbjerg [5] in Fig. 4. We note that there is a general agreement with their result for the final $3d$ state, but not so for the $3s$ final state. This is not unexpected since the use of a pure Coulomb potential for the projectile in the work by Hansen and Taulbjerg can be well justified for *d* states but less so for *s* states; cf. the energies in Table II. This is especially important for collisions at low

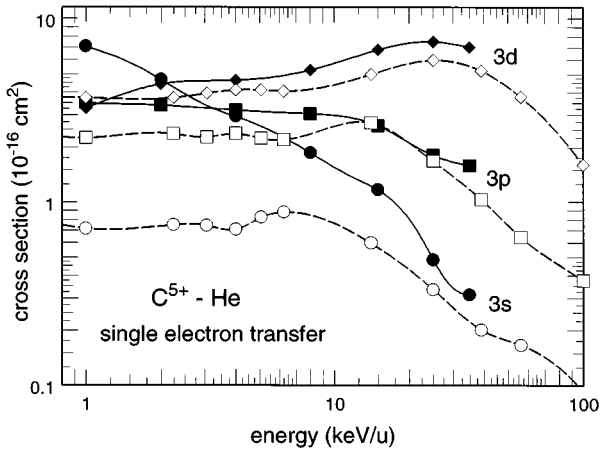

FIG. 4. Calculated cross sections for one-electron transfer in C^{5+}-He collisions to $3s$ (circles), $3p$ (boxes), and $3d$ (diamonds) states. Full symbols designate results from this work, open symbols the corresponding results from the calculation by Hansen and Taulbjerg [5].

TABLE IV. Cross sections, in 10^{-16} cm^2, for line emission after single capture in C^{5+}-He collisions. The data [14] are taken at 4.17 keV/u and the calculated cross sections are at 4 keV/u.

Line	This work	Data [14]	Theory [5]
$2p \rightarrow 1s\ (s)$	1.96	1.40	1.26
$3p \rightarrow 1s\ (s)$	0.76	0.17	0.56
$2p \rightarrow 1s\ (t)$	1.17	0.62	0.56

energies where an accurate representation of the wave functions of the initial and final states is very critical.

There is no experimental data for the single-capture cross sections for this collision system. Suraud *et al.* [14] have measured, at one energy point, a few lines that are emitted from the C^{4+} ion after single-electron capture. Using the branching ratios as given in that work, we derive line emission cross sections $\sigma_{\rm em}$ from the cross sections σ_{nl} in Table III,

$$\sigma^s_{\rm em}(2p\rightarrow 1s) = 0.25(\sigma_{2p}+\sigma_{3s}+\sigma_{3d}), \tag{16}$$

$$\sigma^s_{\rm em}(3p\rightarrow 1s) = 0.25\times 0.952\sigma_{3p}, \tag{17}$$

$$\sigma^t_{\rm em}(2p\rightarrow 1s) = 0.75\times 0.34(\tfrac{1}{3}\sigma_{2p}+\sigma_{3s}+\tfrac{1}{3}\sigma_{3d}), \tag{18}$$

where we have assumed (i) a statistical population of singlet (s) and triplet (t) configurations, (ii) a statistical population of the different total angular momentums J for the triplet states, and (iii) neglected cascades from higher states. The coefficient for σ_{3d} is obtained after the line strength for transitions to the $J=1$ component for the $1s2p\ ^3P_1$ line is calculated. Note that the last line is the intercombination line and only the transition from the $J=1$ fine structure level is observed in the experiment. In Table IV we compare the line emission cross sections for these lines from this work, at 4 keV/u, with the results from the measurement [14] and from the calculations by Hansen and Taulbjerg [5]. There is a large deviation between results from this work and the data, particularly striking for the $3p \rightarrow 1s$ line. There are also major deviations between the results from this work and from the other theory [5], mainly due to the larger population of $3s$ states in the calculations of this work. Inclusion of contributions from the transfer-excitation process to the line emission would further increase our estimate of cross sections.

For many other systems, there generally has been close agreement between calculated cross sections for the population of specific nl projectile states and the measured line emission cross sections; cf., e.g., Ref. [15] and references therein. The degree of disagreement in Table IV is hence rather unusual and disturbing. Without further experimentation, with detection of more lines at more energies, the problem is difficult to resolve.

2. Two-electron transfer

The calculated total two-electron transfer cross sections to C^{3+} $2l2l'$ states are given in Fig. 2. Since data are available only relative to the total two-electron transfer cross section, we show the calculated and measured cross section ratios in Fig. 5. There is good qualitative agreement with the calculations by Hansen and Taulbjerg [5] and with the data by Mack [1] and by Holt *et al.* [2]. The two calculations are seen to agree quantitatively at the higher energies where there are no data. At the lower energies, the relative cross sections from this work agree very well with the two sets of data, except for the $2p2p\ D$ final state where the results by Hansen and Taulbjerg are closer to the data. Mack estimates the uncertainty of the cross sections in his work as better than 25%, while Holt *et al.* show error bars of about 2%. Hence the cross section ratios from this work would still be in agreement with the data by Mack, but too high when compared to the data by Holt *et al.*

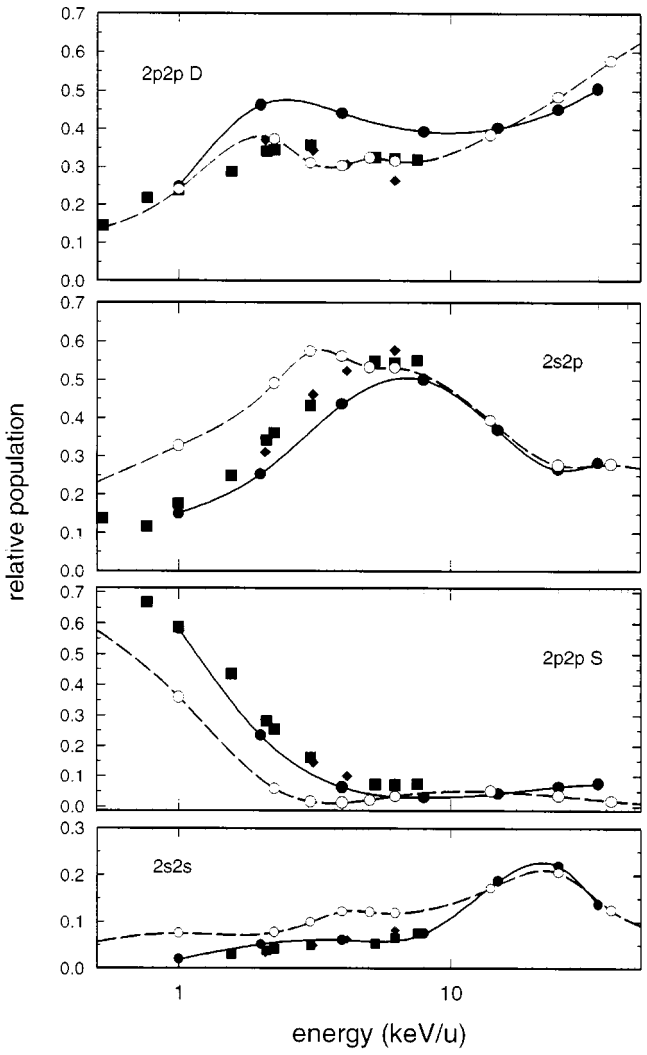

FIG. 5. Relative population of the C^{3+} $nlnl'$ substates in double transfer, derived by dividing the state-selective transfer cross sections by the total two-electron transfer cross section. Shown are the results from this work (full circles), from the calculations by Hansen and Taulbjerg [5] (open circles), and from the measurements by Mack [1] (boxes) and by Holt *et al.* [2] (diamonds).

For the weak transitions to the $2s2s$ and the $2p2p\ S$ states, it appears that the good agreement of the results from this work with the data is rather remarkable, in particular in view of the deviations of the earlier theoretical description

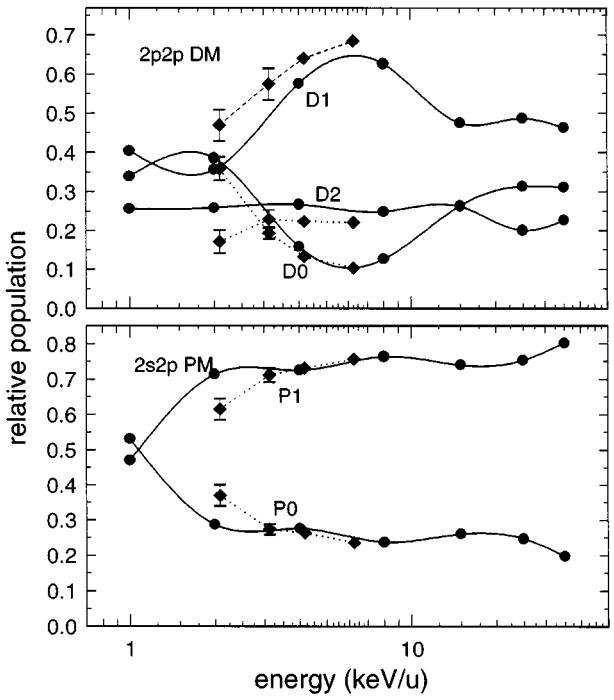

FIG. 6. Relative population of the M substates within the C^{3+} $nlnl'$ manifolds in double transfer. These results represent sub-M cross sections normalized to the total two-electron transfer cross section to all M states within the same L state. Shown are the results from this work (full circles) and from the measurements by Holt *et al.* [2] (diamonds).

[5] by about a factor of 2 or more. For test purposes, we have tried a simpler model in which we include, besides the initial state, only the double-transfer states. It turns out that, at 2 keV/u, the distribution over the $nlnl'$ states from Ref. [5] is closely reproduced by these test calculations. We hence conclude that the better agreement of our results in Fig. 5 with the data is mainly due to the inclusion of the transfer-excitation channel. This channel is, as we have seen earlier in Fig. 3, strong in about the same impact-parameter range where double transfer is strong, but has been left out in Ref. [5].

The calculated distribution over magnetic quantum number M states within a given L shell should provide for an even more sensitive test of the theory. In Fig. 6, we show the normalized cross sections for double transfer to the M substates of the C^{3+} $2s2p$ P and the $2p2p$ D states from this work and from the measurements by Holt *et al.* [2]. The agreement is good qualitatively and even quantitatively. It seems therefore that the model description of the C^{5+}-He system is very satisfactory for two-electron transfer as far as integrated cross sections are concerned.

3. Transfer excitation

In Fig. 7, the calculated cross sections for the population of the C^{4+} $2l$ and the He^{+} $2l$ states, through the process of transfer excitation only, are displayed. Clearly, the population of the C^{4+} $2s$ and $2p$ states through this mechanism is much stronger than the corresponding population through single transfer; cf. Table III.

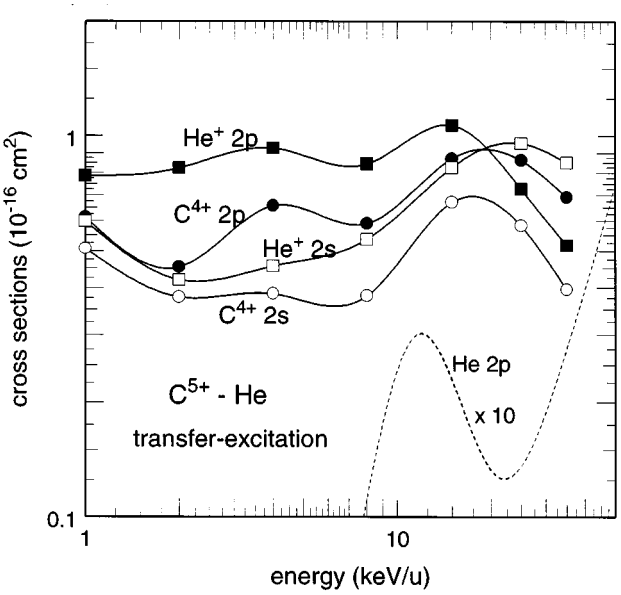

FIG. 7. Calculated cross sections for the population, through the process of transfer excitation only, of the C^{4+} $2s$ state (○), the C^{4+} $2p$ state (●), the He^{+} $2s$ state (□), and the He^{+} $2p$ state (■). The dashed line denotes an assessment of He $2p$ population (note the enhancement factor of 10 in the graph) through single excitation; cf. text.

We also include in Fig. 7 an assessment of the single-excitation cross section of He to its $2p$ state. For this we have taken the calculated excitation cross section for C^{6+}-He collisions [16] and scaled it, using the scaling procedure of Janev and Presnyakov [17,18], to the case of a bare incident charge with charge number of 5. Obviously, the single-excitation cross section of He is much smaller in this energy regime than the cross section for populating excited He^{+} states through transfer-excitation.

There are no data nor is there other theoretical information on transfer excitation for C^{5+}-He collisions. The calculated total transfer-excitation cross section for C^{6+}-He collisions is about 1×10^{-16} cm^2 [16] and hence in the same order as in the present system. The same cross section for the Be^{4+}-He system is, however, about a factor of 5 smaller [16]. This strong variation of cross sections with the charge number of the projectile underlines the role that energy levels play in slow collisions. A scaling relation for transfer-excitation cross sections [19] can hence serve only for a first assessment of the magnitude of cross sections.

C. Differential cross sections and coherence parameters

The results presented in the preceding subsection provide information about the transition probabilities to individual final states after the collision. In order to extract information on the scattering *amplitudes*, coherence parameters or the relative phase among degenerate final states can be obtained from the characteristics of photons or electrons that are emitted from these states. For a single-electron-capture process, the most detailed experimental study possible is the measurement of the polarization and/or the angular distribution of photons emitted in coincidence with the scattered particle. For a double-electron-capture process, on the other hand, it is

the measurement of the anisotropic electron angular distribution from the autoionization of the doubly excited states in coincidence with the angle of the scattered particle. For the present collision system, there is no such ''complete'' measurement for the single-electron-capture process. Such measurements have been performed rather for B^{3+}-He collisions [21,22], where the phase information for electron capture to the dominant $2p$ state has been examined both experimentally and theoretically. For the double-capture process in C^{5+}-He collisions, however, the complex ampitudes for the $2s2p\ ^1P$ and the $2p2p\ ^1D$ states at 25 keV have been studied experimentally [3].

1. Coherence parameters for single transfer to 3p states

Before discussing the differential cross sections and the phase information for the double-capture channels, we first discuss the corresponding results for *single-electron* capture to the $3p$ state at 2 keV/u. The single-capture channel is the dominant channel and its phase information should be examined first in order to compare it with the results for the weaker double capture channels.

In Fig. 8 we show the differential cross section, the fractional population λ_0 [Eq. (10)] of the $3p_0$ state, the orientation parameter $L_\perp$ [Eq. (13)], and the sine of the relative phase angle $\sin\beta_{01}$. The differential cross section is strongly forward peaked, with maximum near 0.16 mrad and dies out at about 0.50 mrad. It also exhibits oscillatory structure that is typically of differential cross sections at low energies.

The fraction λ_0 of the $3p_0$ state, as shown in Fig. 8, is about one-half in the region where the differential cross section peaks. The structures at larger angles have probably little physical significance since the transition probabilties are small and thus are prone to limitations in the theoretical model. The total integrated cross section for $3p_0$ is 1.74×10^{-16} cm^2 and for the sum of $3p_1$ and $3p_{-1}$ states it is 1.59×10^{-16} cm^2.

The differential orientation parameter $L_\perp$ in Fig. 8 is negative and close to -1 in the angular range where the differential cross section is large. Also the corresponding orientation parameter at large impact parameters (not shown) is negative and close to -1. This is consistent with the general propensity rule for orientation parameters in electron-capture processes between multiply charged ions and atoms [20]. This propensity rule is a consequence of the electron following the rotation of the internuclear axis during the collision. Negative orientation parameters at small angles (or large impact parameters), with values close to -1, have also been observed for the $2p$ states that are populated in B^{3+}-He collisions [21].

The phase difference β_{01} between the $m=0$ and $m=1$ amplitudes lacks an obvious physical interpretation even though it is related to the alignment angle. It is shown here for reference further below when the results for double capture to $2s2p\,^1P$ states are discussed.

2. Coherence parameters for double capture to 2s2p ^{1}P

The calculated differential cross sections and coherence parameters for the $2s2p\ ^1P$ state from double capture, in 2 keV/u C^{5+} on He collisions, are shown in Fig. 9. In comparison to single-electron capture, this is a weak channel.

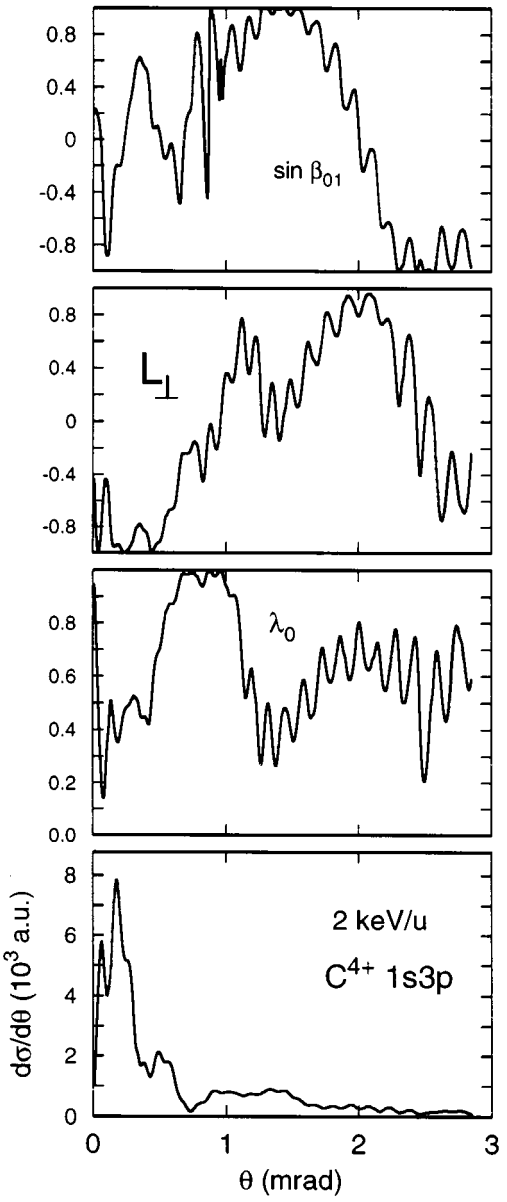

FIG. 8. Calculated dependence on the projectile angle θ of the differential cross section for populating the C^{4+} $1s3p$ state at 2 keV/u, the fractional population λ_0 of the P_0 substate, the orientation parameter $L_\perp$, and the sine of the relative phase angle β_{01}.

The total cross section for the $M=0$ component is 1.25×10^{-17} cm^2 for the sum of the $M=+1$ and $M=-1$ components the cross section is 3.14×10^{-17} cm^2. The differential cross section has the peak near 3 mrad and the transition occurs at much larger angles in comparison with the single-capture process. This is already evident in Fig. 3 from the impact-parameter dependence of these probabilities. The coherence parameters exibit numerous rapid variations at certain narrow angular ranges. When comparing with the differential cross sections, one notes that such seemingly erratic structures occur when the differential cross sections are small and the extracted phase information is less reliable. The significance of these sharp structures is further reduced when an experimental resolution is taken into account.

We note that the propensity rule of a negative orientation parameter is not seen for this double-capture channel. This is

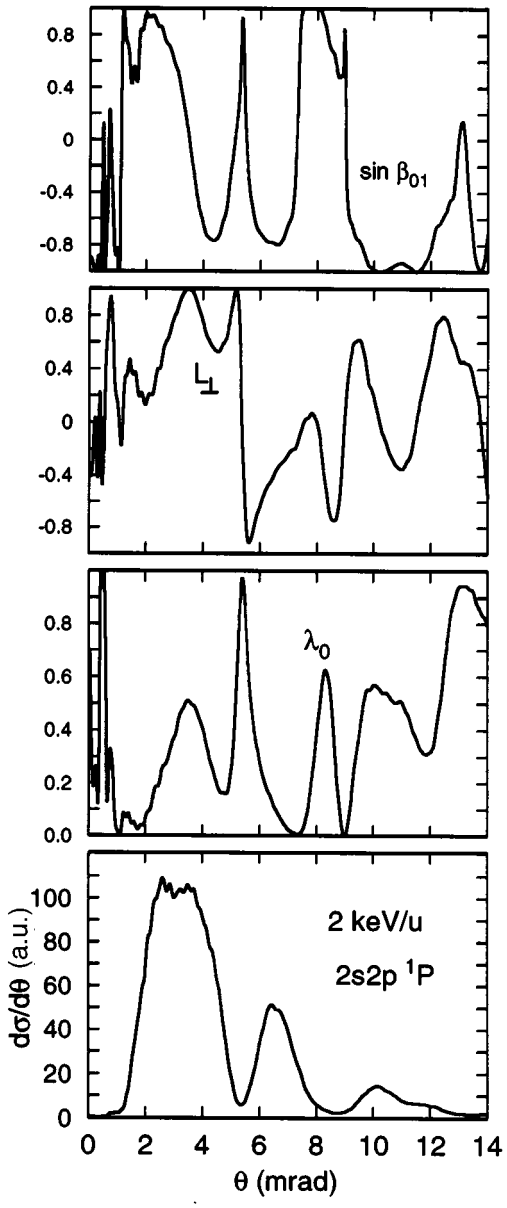

FIG. 9. Calculated dependence on the projectile angle θ of the differential cross section for populating the C^{3+} $2s2p$ ^1P state at 2 keV/u, fractional population λ_0 for the $^1P_0$ substate, orientation parameter $L_\perp$, and the sine of the relative phase angle β_{01}.

not unexpected since double capture occurs at small impact parameters and it is a weak channel. In a previous theoretical study for double capture in Ne^{8+}-He collisions, the $3f^2$ ^1F state is shown to be predominantly populated and strongly oriented [23]. In this case, the $3f^2$ ^1F state is populated at *large* impact parameters and the propensity rule can hence still be applied. The orientation of this state is expected to be close to -4.0.

In order to compare the calculated results in Fig. 9 with measurements, the calculated quantitites should be convoluted with the angular resolution of the experiment. We choose a Gaussian width of 1.2 mrad, which is close to the resolution of the experiment of Khemliche *et al.* [3].

The Gaussian convoluted cross sections and coherence parameters are shown in Fig. 10 and compared there with the experimental results. The calculation of the Gaussian average for the differential cross sections and the fraction λ_0 is straightforward. However, the procedure for calculating the Gaussian average for $\sin\beta_{01}$ needs some explanations. Experimentally this parameter is extracted from measuring the angular distribution of the emitted electron in coincidence with the scattered projectiles. The electron yield is, up to an overall normalization,

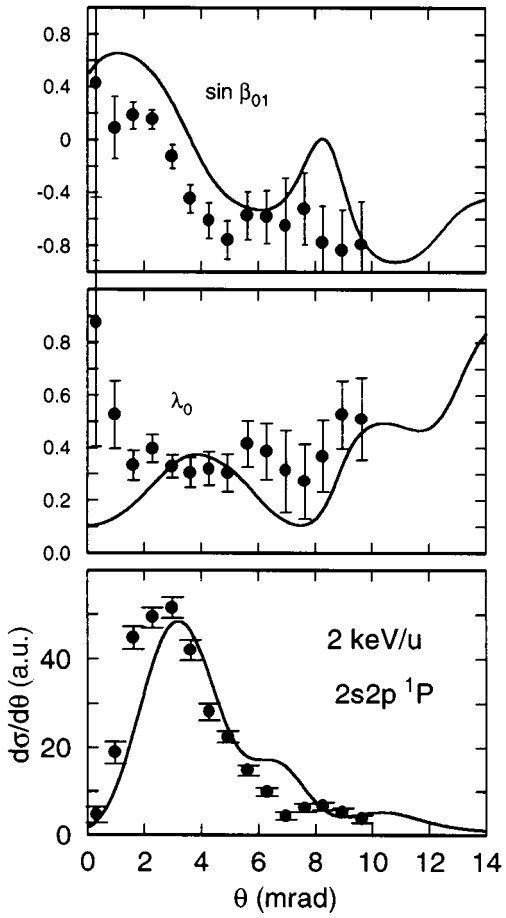

FIG. 10. Same as in Fig. 9, but the calculated results have been smoothed with a Gaussian shaped angle resolution of 1.2 mrad width. Data (full symbols) are from Ref. [3] for 25 keV.

$$S_p(\theta,\theta_e,\phi_e)=|A_1|^2(\sin^2\theta_e)(1-\cos2\phi_e)+|A_0|^2\cos^2\theta_e - |A_1||A_0|\sqrt{2}\sin2\theta_e\sin\phi_e\sin\beta_{01}, \quad (19)$$

where electrons are measured at angles θ_e, ϕ_e within a small solid angle. Thus, to calculate the average of $\sin(\beta_{01})$ we first perform the Gaussian average of $|A_0||A_1|\sin(\beta_{01})$ and then divide the result by the Gaussian average of $|A_0|$ and $|A_1|$.

By and large, the agreement between the calculated and measured results in Fig. 10 is reasonable. Most of the structures in the results of Fig. 9 are gone after performing the Gaussian average. The structures in the calculation can be put to a closer test only if experiments with a finer angular resolution are executed. At the present stage of comparison, the close-coupling description is seen to provide for adequate predictions of the coherent parameters for the weak channels.

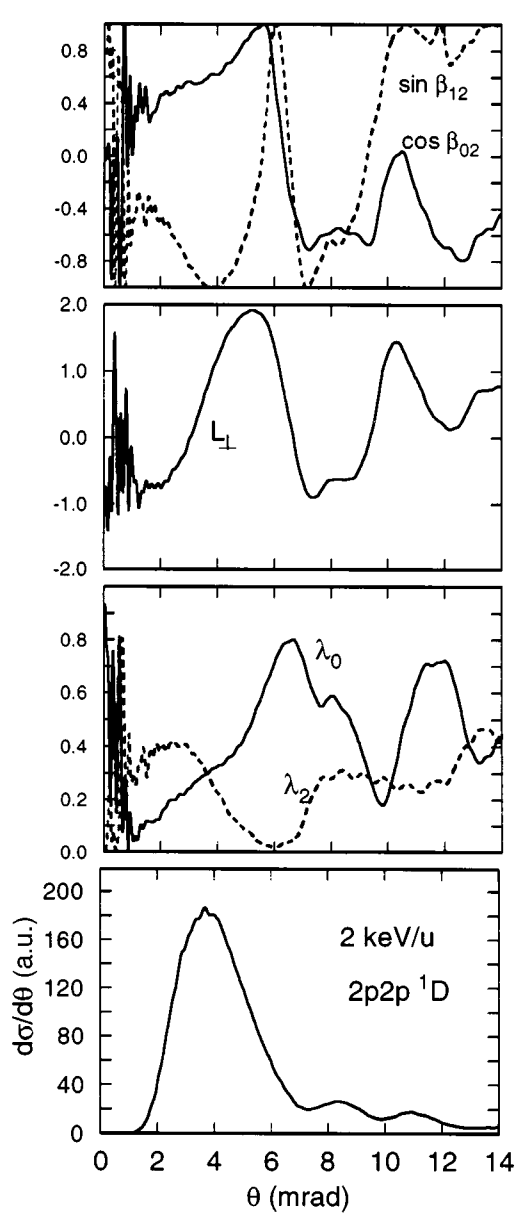

FIG. 11. Calculated dependence on the projectile angle θ of the differential cross section for populating the C^{3+} $2p2p$ ^1D state at 2 keV/u, the normalized probabilities λ_0 and λ_2 for, respectively, the $^1D_0$ and $^1D_2$ substates, the coherence parameter $L_\perp$, the cosine of the relative phase angle β_{02} (solid line), and the sine of β_{12} (broken line).

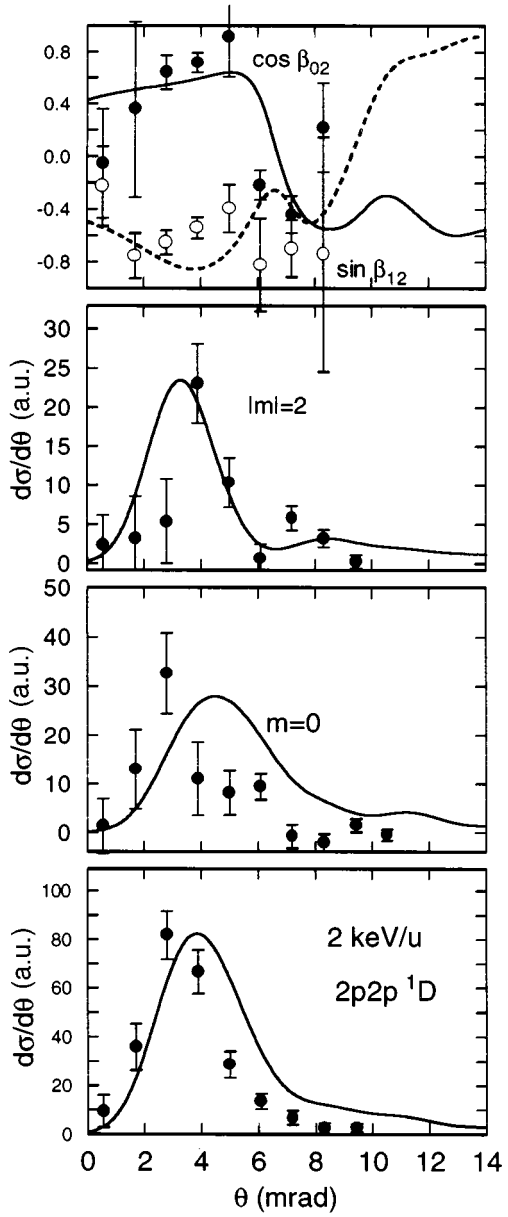

FIG. 12. Same as in Fig. 11, but the calculated results are smoothed with a Gaussian shaped angle resolution of 1.2 mrad width. Data (symbols with error bars) are from Ref. [3].

We do not present here a Gaussian average for the orientation parameter $L_\perp$ since this parameter was not directly measured.

3. Coherence parameters for two-electron transfer to 2p2p ^1D

The differential cross section, the fractions λ_0 and λ_2 of, respectively, $M=0$ and $|M|=2$ substates, the orientation parameter $Ł_\perp$, and $\sin\beta_{01}$ and $\cos\beta_{02}$ similar to those defined in Khemliche *et al.*, are shown in Fig. 11. Similar to the case of the $2s2p$ ^1P state, the rapid oscillations for the coherence parameters at small angles are probably not real since at these small angles the cross sections are rather small. In general we should not attach much physical significance to the results when the differential cross sections are very small.

In order to compare with data we performed the Gaussian convolution with an angular resolution of 1.2 mrad. The resulting differential cross sections and coherence parameters are shown in Fig. 12 together with the data [3]. The differential cross sections and the magnetic substate populations are all in reasonable agreement with experiment. Even the two relative phases are in good agreement with the measurement, except at large angles where the experimental uncertainty is large.

IV. SUMMARY AND CONCLUSIONS

After quite a few theoretical studies of two-electron systems in the past ten years, it is now well established that the

semiclassical close-coupling description is able to predict total and partial cross sections in collisions at low and intermediate energies [7,15]. This is confirmed in this work, which takes into account the electron-electron interaction explicitly for the weak two-electron transfer channels in C^{5+}-He collisions for which there are data from two independent experiments. The agreement with these sets of data is remarkably good (i) for the relative partial cross sections in the two-electron transfer channel and (ii) even for the population of the magnetic substates within states with $L \neq 1$. One would expect that the calculated cross sections for the strong single-transfer channels are even more reliable even though there is disagreement with the very limited data base, one measurement at one energy point. There are also discrepancies with an earlier calculation [5], which we believe are due to the improved representation of the 1*s* core of the projectile in this work, as well as the inclusion of transfer-excitation channels in this work.

In this work we also show that the measured [3] dependence of transfer probabilities and coherence parameters on the projectile scattering angle, for the two measured two-electron transfer channels, can be well reproduced by the calculations when the experimental angular resolution is included. The determination of such details of the electron dynamics in slow collisions, as well as the phase-dependent coherence parameters, has not been attempted before, as far as we know, with atomic-orbital or with molecular-orbital expansions. The challenge by the recent experiment [3] was needed to initiate such a step. We find that for these very weak channels a qualitative understanding of the calculated angular dependencies is rather difficult, if not impossible. Notably, the well-known propensity rule does not seem to apply for the calculated orientation parameter $L_{\perp}$.

ACKNOWLEDGMENTS

We gratefully acknowledge support by the National Institute for Fusion Science Nagoya, Japan, where, with generous local support by H. Tawara, a major portion of the numerical calculations were performed remotely. C. D. L. is partially supported by the National Research Council of Taiwan and by the U.S. Department of Energy, Office of Basic Energy Research, Division of Chemical Sciences, under Grant No. NSC85-2811-M009-004.

[1] E.M. Mack, Ph.D. thesis, Rijksuniversiteit te Utrecht, 1987 (unpublished).
[2] R.A. Holt, M.H. Prior, K.L. Randall, R. Hutton, J. McDonald, and D. Schneider, Phys. Rev. A **43**, 607 (1991).
[3] H. Khemliche, M.H. Prior, and D. Schneider, Phys. Rev. Lett. **74**, 5013 (1995).
[4] W. Fritsch and C.D. Lin, Phys. Rev. A **45**, 6411 (1992).
[5] J.P. Hansen and K. Taulbjerg, Phys. Rev. A **47**, 2987 (1993).
[6] C. Harel and H. Jouin, Europhys. Lett. **11**, 121 (1990).
[7] W. Fritsch and C.D. Lin, Phys. Rep. **202**, 1 (1991).
[8] P.P. Szydlik and A.E.S. Green, Phys. Rev. A **9**, 1885 (1974).
[9] W. Fritsch and C.D. Lin, Phys. Rev. Lett. **61**, 690 (1988).
[10] S. Bashkin and J. Stoner, Jr., *Atomic Energy-Level and Grotrian Diagrams* (North-Holland, Amsterdam, 1978), Vol. I.
[11] T.G. Winter, Phys. Rev. A **38**, 1612 (1988).
[12] A. Dubois, S.E. Nielsen, and J.P. Hansen, J. Phys. B **26**, 705 (1993).
[13] T. Iwai, Y. Kaneko, M. Kimura, N. Kobayashi, S. Ohtani, K. Okuno, S. Takagi, H. Tawara, and S. Tsurubuchi, Phys. Rev. A **26**, 105 (1982).
[14] M.G. Suraud, R. Hoekstra, F.J. de Heer, J.J. Bonnet, and R. Morgenstern, J. Phys. B **24**, 2543 (1991).
[15] W. Fritsch, in *Review of Fundamental Processes and Applications of Atoms and Ions*, edited by C.D. Lin (World Scientific, Singapore, 1993), p. 239.
[16] W. Fritsch, Nucl. Instrum. Methods Phys. Res. Sect. B **98**, 246 (1995).
[17] R.K. Janev and L.P. Presnyakov, J. Phys. B **13**, 4233 (1980).
[18] W. Fritsch and K.-H. Schartner, Phys. Lett. A **126**, 17 (1987).
[19] W. Fritsch, Phys. Lett. A **192**, 369 (1994).
[20] M. Lundsgaard and C.D. Lin, J. Phys. B **25**, L429 (1992).
[21] P. Roncin, C. Adjouri, N. Andersen, M. Barat, A. Dubois, M.N. Gaboriaud, J.P. Hansen, S.E. Nielsen, and S.Z. Szilagyi, J. Phys. B **27**, 3079 (1994).
[22] C. Adjouri, P. Roncin, M.N. Gaboriaud, M. Barat, and N. Andersen, J. Phys. B **27**, 3093 (1994).
[23] Z. Chen and C.D. Lin, Phys. Rev. A **48**, 1298 (1993).